Analyst

Molecular evidence of toxic effect on the biofilm and its matrix

Journal:	*Analyst*
Manuscript ID	AN-COM-12-2018-002512.R1
Article Type:	Communication
Date Submitted by the Author:	21-Jan-2019
Complete List of Authors:	Ding, Yuanzhao; Nanyang Technological University, School of Civil and Environmental Engineering Zhou, Yufan; Pacific Northwest National Laboratory, W. R. Wiley Environmental Molecular Science Laboratory Yao, Juan; Pacific Northwest National Laboratory , Atmospheric Sciences and Global Change Division Qiong, Yijia; Western Univ. Health Zhu, Zihua; Pacific Northwest National Laboratory , Environmental Molecular Sciences Laboratory Yu, Xiao-Ying; Pacific Northwest National Laboratory , Atmospheric Sciences and Global Change Division

Analyst

COMMUNICATION

Molecular evidence of toxic effect on the biofilm and its matrix

Yuanzhao Ding[a,b], Yufan Zhou[c], Juan Yao[a], Yijia Xiong[d], Zihua Zhu*[c], and Xiao-Ying Yu*[a]

Received 00th January 20xx,
Accepted 00th January 20xx

DOI: 10.1039/x0xx00000x

www.rsc.org/

Shewanella oneidensis MR-1 wild-type and a hyper-adhesive mutant CP2-1-S1 are used as model organisms and Cr (VI) selected as a toxic chemical to study biofilm and toxic chemical interactions. Biofilms are cultured in a microfluidic device for in situ time-of-flight secondary ion mass spectrometry imaging. This approach is viable for studying biofilms' responses to antimicrobial resistance.

Micro-organisms prefer to attach onto the surfaces or interfaces and build up their structures or biofilms in the natural and engineered environments. The biofilm is a group of micro-organisms on the surfaces (or interfaces), embedded with a self-produced extracellular polymeric substance (EPS).[1] The surfaces or interfaces are important to bacteria attachment leading to biofilm formation; and the biofilm is important to the environment. The biofilm is ubiquitous and can be found in many places (e.g., the surface of medical devices and natural environment).[2] One key challenge of biofilms is the EPS matrix. The main components of EPS are proteins, polysaccharides, extracellular DNAs, and lipids. The EPS works as the matrix of the bacteria cells.[3] Toxic chemicals, such as Cr (VI) in the form of $Cr_2O_4^{2-}$, can affect the stability of biofilm and the EPS matrix,[4] while the biofilm and EPS matrix can also respond to environmental perturbation. However, the details of such mechanism are still unclear.

To study the repsonse of biofilm and its EPS matrix to external perturbations, chemical information with higher resolution in living systems is strongly needed. *Shewanella oneidensis* MR-1 cells are generally 1 µm wide and several µm long. Although probing the bacteria cell and its associated matrix using bulk approaches give some chemical information, they fail to differentiate whether the effect is from the bacteria or the EPS. Many methods have been used to study the chemical information of the EPS matrix including liquid chromatography-mass spectrometry (LC-MS) [5] for chemical compositions of the biofilm, a phenol-sulfuric acid method for quantification of total carbohydrates [6], and bicinchoninic acid assay for proteins) [7]. Direct chemical mapping (e.g., Matrix-assisted laser desorption/ionization, MALDI) was used to examine the biological samples.[8] However, the approaches mentioned above requires extraction or other sample pre-treatment before analysis and these processes might negatively affect the biofilm structure during analysis. Mass spectrometry needs a vacuum environment, making it difficult to analyze live biofilms directly. We recently demonstrated that a novel microreactor, System for Analysis at the Liquid Vacuum Interface (SALVI), can be used to introduce living biofilms to advanced spectrometry and microscopy.[9-11] Specifically, the SALVI microreactor coupling with time-of-flight secondary ion mass spectrometry (ToF-SIMS) permits *in situ* dynamic molecular imaging of live biofilms, providing submicron mapping to distinguish the chemical distribution of biofilms and potentially elucidate the mechanism of how toxic chemicals affect the biofilm and its matrix.

S. oneidensis is capable of electron transfer [12], and has diverse applications ranging from microbial fuel cells for electricity generation[13] to contaminant removal.[14, 15] However, the Cr (VI) will cause the biofilm to disperse,[4] leading to the lower performance of WT biofilm. To solve this problem, the hyper-adherent mutant CP2-1-S1 (CP) was invented previously, which had a higher biofilm formation capability and formed more robust and cohesive even in Cr(VI) environment when given the same growth condition as WT.[16] However, its mechanism was still unknown. Our recent study successfully used *in situ* ToF-SIMS enabled by SALVI to investigate the main chemical components in the WT biofilm.[11] We employ the same approach to examine the differences of chemical mapping between the WT biofilm and hyper-adhesive mutant CP biofilm in this work. The WT and CP biofilm's responses to the Cr(VI) are compared using in situ live biofilm SIMS imaging. We find: (1) more larger water clusters (possibly gathered by hydrophobic polymers [17, 18]) exist in mutant CP biofilms; (2) polysaccharides are indispensable during biofilm formation, as the more sticky CP biofilm has relatively higher polysaccharides

[a] Earth and Biological Sciences Directorate, Pacific Northwest National Laboratory, Richland, Washington 99354, United States, E-mail: xiaoying.yu@pnnl.gov
[b] Singapore Centre for Environmental Life Sciences Engineering (SCELSE), Nanyang Technological University, 637551, Singapore, E-mail: bincao@ntu.edu.sg
[c] Environmental and Molecular Science Laboratory, Pacific Northwest National Laboratory, Richland, Washington 99352, United States, E-mail: zihua.zhu@pnnl.gov
[d] College of Osteopathic Medicine of the Pacific-Northwest, Western University of Health Sciences, Lebanon, Oregon 97355, USA
Electronic Supplementary Information (ESI) available: [details of any supplementary information available should be included here]. See DOI: 10.1039/x0xx00000x

composition; and (3) more active riboflavin activities in the CP implying that the CP biofilm works harder and generates more quorum sensing molecules (QS, triggering biofilm formation [19, 20]), as a result, the CP biofilm are more responsive to the environmental perturbation.

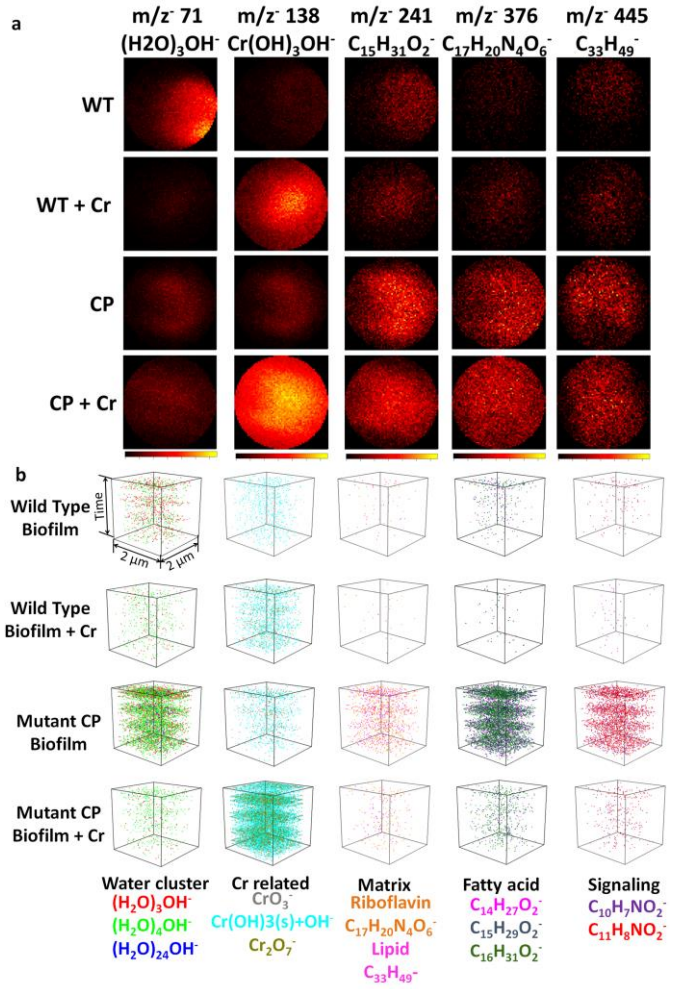

Figure 1. (a) Representative normalized 2D images reconstructed from Region II; (B) normalized 3D chemical mapping of representative water clusters, Cr-related chemicals, riboflavin, lipid, fatty acid, and signalling molecules

Experimental details are presented in the Electronic Supplementary Information. The biofilm development under hydrodynamic conditions in the SALVI microreactor was analysed using structured illumination microscopy (SIM). After growing for seven days, biofilms of the mutant strain CP were well-developed in the microfluidic channel, while the biofilms of the WT were relatively unstructured (see Figure S1. For the Cr (IV) treated samples, the Cr was added into SALVI at the Day 7. The WT biofilm significantly detached 48 hours after Cr treatment, while the mutant CP biofilms were still robust and structured after the same length of time (see Figure S1). This in situ imaging approach characterizes the biofilm attachment surface and the interface is not affected by the biofilm thickness. When analysing dried biofilms, important biological information will be missing. For instance, water clusters will not be observable in dried biofilms.

The SIM observation was consistent with a previous study.[11] The mutant CP exhibited an enhanced capability in biofilm formation under both static and hydrodynamic conditions in an earlier work.[16] At the same time, the CP biofilm had a significant lower detachment rate when exposure to Cr, compared to the WT biofilm.[16]

The fragments of matured untreated biofilms and Cr treated biofilms were analysed by *in situ* liquid ToF-SIMS. Two-dimensional (2D) normalized images of characteristic m/z peaks reconstructed from Region II (Figure S3a) were depicted in Figure 1a. Significant increases in ion count intensities between Region I and Region II (Figure S3a) indicated that the SiN membrane was drilled through in region I, and critical biofilm components (e.g., riboflavin m/z⁻ 376 $C_{17}H_{20}N_4O_6^-$) were found in Region II and Region III. Representative SIMS negative mass spectra of different samples were shown in Figure S3b. SIMS spectra were reconstructed within 200 s after the SiN membrane punch-through (Region III in Figure S3a). In the positive spectra, many interesting peaks were found, including m/z⁺ 159 (polymer, $C_6H_7O_5^+$), m/z⁺ 172, (signalling molecule, $C_8H_{12}NO_3^+$). Similarly, the negative spectra showed many representative peaks, including m/z⁻ 241 (pentadecanoic acid, $C_{12}H_9N_4O_2^-$), m/z⁻ 255 (palmitic acid, $C_{16}H_{31}O_2^-$), m/z⁻ 376 (riboflavin, $C_{17}H_{20}N_4O_6^-$) and m/z⁻ 455 (cyclic lipid, $C_{33}H_{49}^-$). The details of possible peak identification are shown in Tables S2-S6.

Considering the complexity of SIMS results, the peaks were identified using the following process: (1) the all peak spectral PCA was performed to identify the major peaks that distinguish all samples; (2) the major peaks found in previous studies of similar biological systems using mass spectrometry[9, 21, 22]; and (3) standard dry and liquid samples analysed to confirm the peaks' identification.[11] Because of the unit mass resolution in liquid SIMS measurement,[23] more than one peak might occur at the same mass to charge ratio (m/z). For example, the peak of m/z⁺ 28 might be the signals from Si^+ [9] or the signal from $C_2H_4^+$, which was a fragment from an organic in positive ion mode [24]. In this case, we used the most likely peak assignment based on the sample's biological characteristics, if not specifically noted.

We used the 2D and three-dimensional (3D) images coupled with spectral PCA and image PCA to investigate how water clusters were changed depending on the type of biofilms. The PCA peak selection criteria were based on the following: (1) the peak intensity was higher than 0.5% of total intensity; (2) the peak intensity was higher than its neighbouring peaks; and (3) the peak represented important biofilm chemical components. The selected peaks were normalized to the total ion intensity of the selected peaks followed with square root transformation and mean cantering before running the spectral PCA.[11] In the spectral PCA result in the positive ion mode, PC3 separated the mutant CP biofilm and WT biofilm (Figure S7). The majority of water clusters $(H_2O)_nH^+$, n =1, 5, 8-11, 13-21, 23-27, 29-33, 35, 37, 38, 41, 43 from PC3 negative loadings were more characteristic for mutant biofilms. In the range of large water clusters $(H_2O)_nH^+$ $n \geq 8$, most of the peaks had negative loadings, suggesting that the CP biofilms tend to form larger water clusters. Most of the small water clusters $(H_2O)_nH^+$ $n \leq 7$ showed

an opposite trend, indicating that the WT biofilm was more likely to form smaller water clusters (see PC3 in Figure S7). Such an observation suggests that the water environment in the CP biofilm is more hydrophobic than the WT.[11] In addition, we noticed that the CP biofilm formed a more cohesive and thicker biofilm compared to the WT biofilm.[16] Therefore, an explanation is that the CP biofilm may contain more EPS components (e.g., proteins, polysaccharides, extracellular DNAs, lipids). The latter organic molecules may form a thin layer on the CP biofilm biointerface, modifying the surrounding water environment and leading to the formation of larger water clusters compared to the WT biofilm (Figure 1). In addition, a previous study showed that the bacterial surface charges and hydrophobicity might have a crucial impact on cells' initial attachment to the surface or interface [25]. It has been postulated that a relatively higher hydrophobicity might lead to denser biofilms;[26] and our data provide direct molecular evidence to support this earlier postulation.

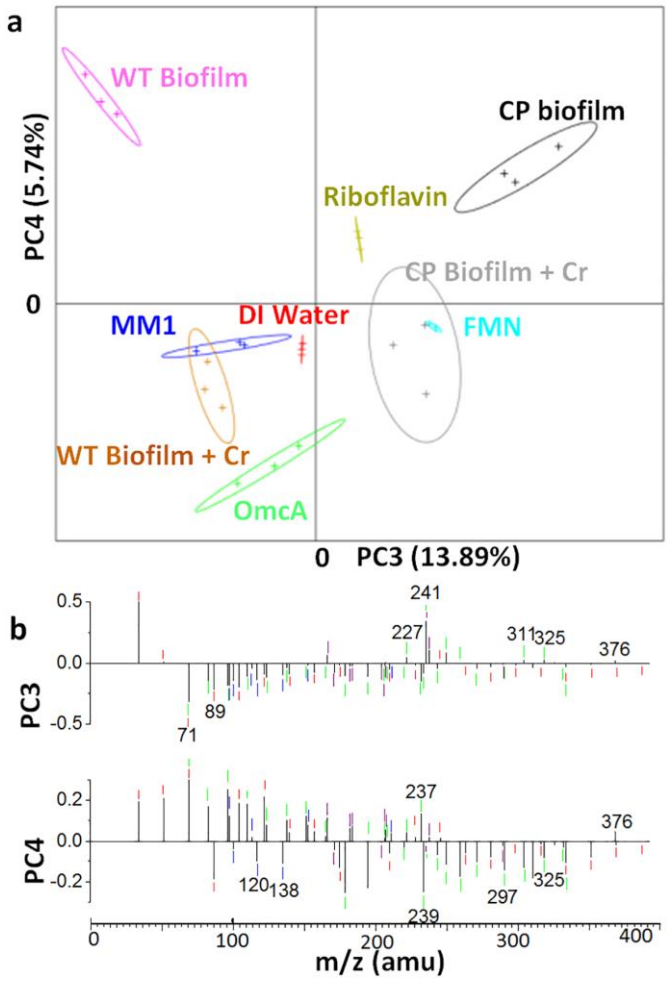

Figure 2. Spectral PCA in the negative mode: (a) PC3 vs. PC4 score plot; (b) loading plots. The red marks indicate water clusters, blue chromium reduction related peaks, purple quorum sensing signal peaks, and green fatty acid peaks. Additional spectral PCA results are in Figures S7 and S8.

S. oneidensis cells with higher hydrophobic were reported to have better adhesion to the graphite electrode.[27] The CP biofilm was associated with larger water clusters indicating a higher hydrophobic environment. The fact that the water clusters between the WT and CP biofilms are different suggests that the water property is biologically modified by the CP biofilm more toward building a thicker biofilm, leading to possibly a higher efficiency in electricity generation by the microbial fuel cell [28] or higher capability in contaminant removal [4].

In SIMS negative spectra, several fatty acid peaks were found to contribute to the separation between the mutant and WT strains including m/z$^-$ 199 (lauric acid $C_{12}H_{23}O_2^-$), m/z$^-$ 213 (tridecylic acid $C_{13}H_{25}O_2^-$), m/z$^-$ 227 (myristic acid $C_{14}H_{27}O_2^-$), m/z$^-$ 241 (pentadecanoic acid $C_{15}H_{29}O_2^-$), and m/z$^-$ 255 (palmitic acid $C_{16}H_{31}O_2^-$). The negative spectral PCA results showed that fatty acid peaks were more predominant in the CP biofilm than the WT biofilm. For example, PC3 separated the CP biofilm and WT biofilm (Figure 2a). The peaks of m/z$^-$ 227 (myristic acid $C_{14}H_{27}O_2^-$) and m/z$^-$ 241 (pentadecanoic acid $C_{15}H_{29}O_2^-$) were two significant peaks that contributed to this separation (Figure 2b). When looking in the reconstructed 2D and 3D images, the signal from m/z$^-$ 241 (pentadecanoic acid $C_{15}H_{29}O_2^-$) was higher in the CP biofilm than the WT biofilm (Figure 2).

In the positive spectral PCA results, PC3 separated the CP biofilm and the WT biofilm. Several cyclic lipids were major contributors to the separation, including m/z$^+$ 413 ($C_{28}H_{45}O_2^+$), m/z$^+$ 429 ($C_{29}H_{49}O_2^+$), m/z$^+$ 469 ($C_{28}H_{21}MgN_4O_2^+$), and m/z$^+$ 485 ($C_{28}H_{21}MgN_4O_3^+$) (Figure S6) The positive spectral PCA results showed that cyclic lipids' peaks were more dominant in the CP biofilm, suggesting CP biofilm had more lipids and formed more cohesive biofilms. The positive 2D image PCA results showed a global effect after Cr(VI) perturbation (Figure S9). The first three PCs explained 74.85% of the variance. For PC1, the strongest positive loading fragments were the PQS molecule m/z$^+$ 175 ($C_{10}H_9NO_2^+$) and palmitic acid m/z$^+$ 239 ($C_{16}H_{31}O^+$) depicted in bright red areas in PC1 (Figure S9). Other significant peaks included m/z$^+$ 261 chlorine-containing polymers ($C_{15}H_{11}Cl_2^+$), m/z$^+$ 453 cyclic lipid ($C_{28}H_{21}MgN_4O^+$), and m/z$^+$ 509 microbial mat-diacylglycerol ($C_{32}H_{41}O_4^+$) (Figure S9). PC1 explained 61.65% of the variance. The PC1 images of the WT biofilm and the CP biofilm were brighter, suggesting that these two groups had a relatively higher signaling molecule and fatty acid components. After Cr(VI) addition, the PC1 image of the WT and Cr area was dark red, and the PC1 image of CP and Cr areas bright red (Figure S9). This suggested that as the WT biofilm dispersed due to Cr (VI) exposure, key matrix components became less important. On the contrary, the CP mutant was strong enough to sustain the Cr (VI) attack. Consequently, the matrix components were reduced, however, not totally diminished in the WT biofilm.

Lipids were one of the major components of the biofilm matrix, and it encompassed small molecules such as fatty acids and their derivatives.[1, 29, 30] Therefore, fatty acids played a crucial part in biofilm development. Our data show higher fatty acid signals in the CP biofilm, suggesting that the mutant biofilm had a higher lipid production and higher biofilm formation capability. This is consistent with our SIM observation (CP biofilm was more cohesive and robust), in agreement with a previous study that showed that CP biofilms had a higher viscosity than the WT biofilm.[16] Lipids might provide the

structural support and viscosity to form the biofilm matrix. Our results provide a more direct observation of matrix components, specifically cyclic lipids, indicating that the CP biofilm is more robust and cohesive by higher cyclic lipid contents.

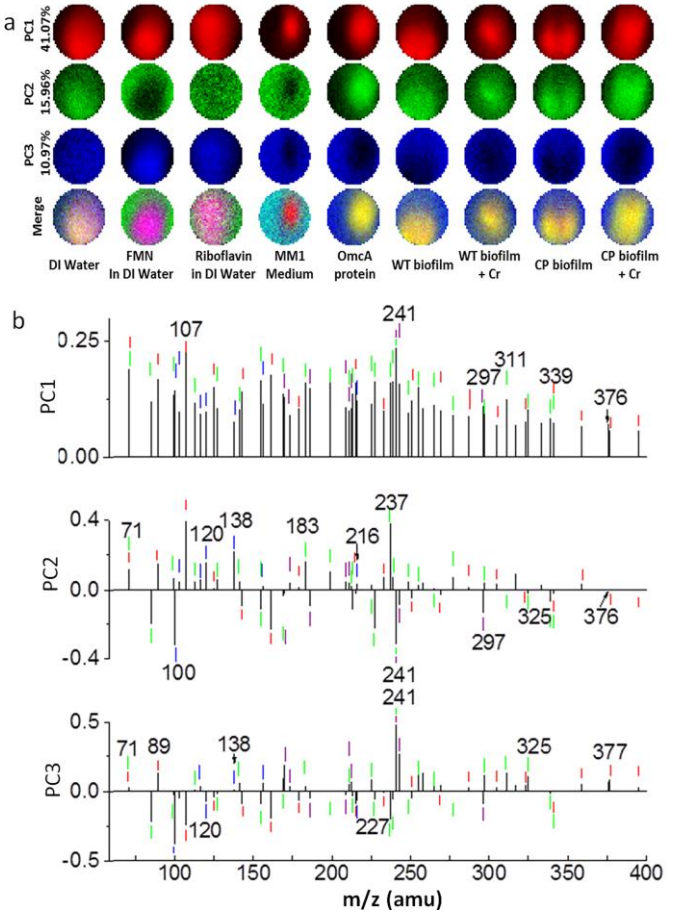

Figure 3. Image PCA in the negative ion mode: (a) Reconstructed false-colour 2D PCA images in RGB corresponding to each PC scores at these locations along the microfluidic channel. The RGB composite images of the three key PCs are depicted. (b) Only data within the 2 µm diameter circle were considered in the analysis; Image PCA loading plots illustrating the contribution of the selective chemical species. The brighter colour indicates positive loadings and darker negative loadings. Image PCA in positive ion mode can be found in Figure S9.

Riboflavin plays a significant role in extracellular electron transfer in *S. oneidensis* MR-1 [31]. The two main positive peaks for riboflavin were m/z$^+$ 243 ($C_{12}H_{11}N_4O_2^+$) and m/z$^+$ 377 ($C_{17}H_{21}N_4O_6^+$); and the two main negative peaks were m/z$^-$ 241 ($C_{12}H_9N_4O_2^-$) and m/z$^-$ 376 ($C_{17}H_{20}N_4O_6^-$). In the positive mode, PC3 separated the CP biofilm and the WT biofilm; and m/z$^+$ 243 $C_{12}H_{11}N_4O_2^+$ and m/z$^+$ 377 $C_{17}H_{21}N_4O_6^+$ were crucial contributors (Figure S7). Similarly, the PC3 separated the CP biofilm and the WT biofilm in negative spectral PCA, while the peaks of m/z$^-$ 241 $C_{12}H_9N_4O_2^-$ and m/z$^-$ 376 $C_{17}H_{20}N_4O_6^-$ contributed to this separation (Figures 2a and 2b). In 2D images, the CP biofilm had a higher intensity of m/z$^-$ 376 ($C_{17}H_{20}N_4O_6^-$), compared to the WT biofilm (Figure 1a). As a result, the CP biofilm had a relatively higher riboflavin production than the WT biofilm.

Our SIMS results verify that CP biofilm produces more riboflavin, a co-respondent in the microbial fuel cell,[28] providing more evidence of higher riboflavin amount in the CP biofilm for electron transfer. A previous study showed that the riboflavin might act as electron shuttles in electricity generation,[32] and the CP biofilm can produce more electricity compared to the WT biofilm.[28] The ability to monitor riboflavin in the biofilm helps elucidation of the electron shuttling process for more applications of the biofilm in microbial fuel cells.

Specifically, negative 2D and 3D images showed a similar trend. For example, the signals of m/z$^-$ 241 (pentadecanoic acid, $C_{12}H_9N_4O_2^-$), m/z$^-$ 376 (riboflavin, $C_{17}H_{20}N_4O_6^-$) and m/z- 445 (cyclic lipid, $C_{33}H_{49}^-$) were much stronger in the CP biofilm with Cr addition compared to the WT biofilm under Cr attack (Figure 3a). The 2D images were consistent with the image PCA result, supporting that the Cr(VI) had a more significant toxic effect on the WT biofilm than the CP biofilm.

Furthermore, relevant biomarkers indicative of QS were observed in *S. oneidensis* MR-1 in this work. In the positive spectral PCA, PC3 separated the CP biofilm and the WT biofilm. The peaks of N-butyryl-L-Homoserine lactone m/z$^+$ 172 ($C_8H_{13}NO_3^+$) and a fragment of quinolone molecule m/z$^+$ 175 ($C_{10}H_9NO_2^+$) were two of the largest contributors (Figure S7). N-butyryl-L-Homoserine lactone m/z$^+$ 172 ($C_8H_{13}NO_3^+$), also known as C4-HSL, played a crucial role in biofilm development in *Pseudomonas aeruginosa*.[33, 34] The m/z$^+$ 175 ($C_{10}H_9NO_2^+$) was identified as a *P. aeruginosa* Quinolone Signal (PQS), an important molecule in biofilm formation. This peak was identified as a PQS peak in another SIMS study.[35]

For QS molecules, N-butyryl-L-Homoserine lactone m/z$^+$ 172 ($C_8H_{13}NO_3^+$) and a fragment of quinolone molecule m/z$^+$ 175 ($C_{10}H_9NO_2^+$) are two of the largest contributors to *Pseudomonas aeruginosa* biofilm formation. Since m/z$^+$ 172 and m/z$^+$ 175 contribute more to the positive PC3 (Figure S7) and higher signals of m/z$^+$ 172 and m/z$^+$ 175 were observed in 2D and 3D images of the CP biofilm (Figure S4b and S4c), we propose that the CP biofilm might also synthesize more C4-HSL and quinolone in the biofilm formation process. The higher concentration of C4-HSL and quinolone can lead to higher biofilm formation capability. Consequently, such property might be used in bioengineering (e.g., carbon removal by the bioreactors [36]) in the future.

In addition, PC4 scores decrease after Cr treatment for both the WT and CP biofilms, while PC3 scores only slightly shift (Figure 2). The PC4 loading shows two characteristic negative signals, m/z$^-$ 120 $Cr(OH)_3(s)+OH^-$ and m/z$^-$ 138 $Cr(OH)_3(s).H_2O+OH^-$, suggesting that $Cr_2O_7^-$ can be reduced by both biofilms.

The reconstructed 3D images showed that Cr (VI) can be reduced to Cr(III) as m/z$^-$ 120 $Cr(OH)_3(s)+OH^-$ or m/z$^-$ 138 $Cr(OH)_3(s).H_2O+OH^-$ in the biofilm (Figure 1b) [11]. However, the performances between WT and CP biofilm differed. For example, the CP biofilm reduced almost all Cr(VI) to Cr (III). This was visualized by the high m/z$^-$ 120 $Cr(OH)_3(s)+OH^-$ and low m/z 216 $Cr_2O_7^-$ (yellow color) in the 3D images. In the WT biofilm, although signals from m/z$^-$ 120 $Cr(OH)_3(s)+OH^-$ dominated, some m/z 216 $Cr_2O_7^-$ (yellow color) still existed (Figure 1b). The

CP biofilm was more stable when exposed to Cr(VI). At the same time, the CP biofilm could immobilize more Cr(VI) and reduce all Cr(VI) to Cr(III) compared to the WT biofilm under similar conditions [16]. Our image PCA and 3D images were consistent with the previous study; however, direct molecular observation brought more insight that the CP biofilm had a higher efficiency on Cr(VI) immobilization than the WT biofilm.

It was known that Cr(VI) was toxic to bacteria and led to biofilm dispersion [4] and CP biofilm was more robust under the toxic chemical.[16] Our 2D image PCA results show that Cr (VI) significantly affects the WT biofilm (i.e., leading to WT biofilm dispersion), while CP biofilm is not significantly changed. As discussed, stronger signals from lipids, riboflavin, and quorum sensing molecules are found in the sticky CP biofilm, suggesting additional biological functions to resist Cr (VI) toxicity. Considering the Cr(VI) was highly toxic to human health,[37] the CP biofilm with the stronger capability to reduce more Cr (VI) to Cr(III) has a potential in environmental engineering such as water cleaning in the future.

ToF-SIMS coupled with SIM was applied to obtain a submicron spatial molecular mapping of live biofilms. Two different *S. oneidensis* strains, namely, WT and CP biofilms, were used to investigate if the phenome type had any effect on the biofilm's response to external perturbations. A toxic heavy metal ion, Cr(VI), was used as a model of the toxic chemicals. Our findings show the following: (1) water clusters affect the biofilms' robustness and cohesiveness of CP biofilms, which is evidenced by the higher occurrence of larger water clusters; (2) the sticky CP biofilm yield a higher biosynthesis of fatty acids, riboflavin, and QS molecules, leading to higher biofilm formation and sustaining capability; and (3) Cr perturbation seems to affect the stability of the WT biofilm more significantly, while the CP biofilm does not change as much after Cr (IV) treatment. More fatty acids and QS signalling molecules are produced by the CP biofilm, possibly reflecting the proactive nature of the CP biofilm in maintaining the EPS and the overall biofilm integrity in a time of danger.

Conflicts of interest

There are no conflicts to declare.

Acknowledgements

Y. Ding was supported by the research scholarship from Nanyang Technological University. Y. Ding thanked the academic support from Associate Prof. Cao Bin from Nanyang Technological University. Funding for the other authors was from the Pacific Northwest National Laboratory (PNNL) Environmental and Biological Science Directorate (EBSD) Mission seed LDRD. The research was performed in the W. R. Wiley Environmental Molecular Sciences Laboratory (EMSL), a national scientific user facility sponsored by OBER and located at PNNL.

References

1. H. C. Flemming and J. Wingender, *Nature Reviews Microbiology*, 2010, **8**, 623-633.
2. R. M. Donlan, *Emerging Infectious Diseases*, 2002, **8**, 881-890.
3. H. C. Flemming, T. R. Neu and D. J. Wozniak, *Journal of Bacteriology*, 2007, **189**, 7945-7947.
4. B. Cao, P. D. Majors, B. Ahmed, R. S. Renslow, C. P. Silvia, L. Shi, S. Kjelleberg, J. K. Fredrickson and H. Beyenal, *Environmental Microbiology*, 2012, **14**, 2901-2910.
5. C. Pieper, D. Risse, B. Schmidt, B. Braun, U. Szewzyk and W. Rotard, *Water Research*, 2010, **44**, 4559-4569.
6. T. Masuko, A. Minami, N. Iwasaki, T. Majima, S. I. Nishimura and Y. C. Lee, *Analytical Biochemistry*, 2005, **339**, 69-72.
7. M. J. Lim, W. F. Patton, N. Shojaee and D. Shepro, *Molecular Biology of the Cell*, 1995, **6**, 2592-2592.
8. Y. L. Wang, Q. Zhou, B. Li, B. P. Liu, G. X. Wu, M. Ibrahim, G. L. Xie, H. Y. Li and G. C. Sun, *BMC Microbiology*, 2012, **12**, 1-7.
9. X. Hua, X. Y. Yu, Z. Y. Wang, L. Yang, B. W. Liu, Z. H. Zhu, A. E. Tucker, W. B. Chrisler, E. A. Hill, T. Thevuthasan, Y. H. Lin, S. Q. Liu and M. J. Marshall, *Analyst*, 2014, **139**, 1609-1613.
10. X. Hua, M. J. Marshall, Y. J. Xiong, X. Ma, Y. F. Zhou, A. E. Tucker, Z. H. Zhu, S. Q. Liu and X. Y. Yu, *Biomicrofluidics*, 2015, **9**, 031101.
11. Y. Ding, Y. Zhou, J. Yao, C. Szymanski, J. K. Fredrickson, L. Shi, B. Cao, Z. Zhu and X. Y. Yu, *Anal Chem*, 2016, **88**, 11244-11252.
12. J. T. Babauta, H. D. Nguyen and H. Beyenal, *Environmental Science & Technology*, 2011, **45**, 6654-6660.
13. R. B. Jani, P. J. S. Colberg, C. M. Eggleston, L. Shi and C. J. Reardon, *Geochimica Et Cosmochimica Acta*, 2010, **74**, A457-A457.
14. B. Cao, B. Ahmed, D. W. Kennedy, Z. M. Wang, L. Shi, M. J. Marshall, J. K. Fredrickson, N. G. Isern, P. D. Majors and H. Beyenal, *Environmental Science & Technology*, 2011, **45**, 5483-5490.
15. B. Cao, L. A. Shi, R. N. Brown, Y. J. Xiong, J. K. Fredrickson, M. F. Romine, M. J. Marshall, M. S. Lipton and H. Beyenal, *Environmental Microbiology*, 2011, **13**, 1018-1031.
16. Y. Ding, N. Peng, Y. Du, L. Ji and B. Cao, *Appl Environ Microbiol*, 2014, **80**, 1498-1506.
17. L. Infantes and S. Motherwell, *Crystengcomm*, 2002, **4**, 454-461.
18. T. Koddermann, F. Schulte, M. Huelsekopf and R. Ludwig, *Angewandte Chemie-International Edition*, 2003, **42**, 4904-4908.
19. D. G. Cvitkovitch, Y. H. Liu and R. P. Ellen, *Journal of Clinical Investigation*, 2003, **112**, 1626-1632.
20. T. R. de Kievit, *Environmental Microbiology*, 2009, **11**, 279-288.
21. T. Leefmann, C. Heim, A. Kryvenda, S. Siljestrom, P. Sjovall and V. Thiel, *Organic Geochemistry*, 2013, **57**, 23-33.
22. T. Leefmann, C. Heim, S. Siljestrom, M. Blumenberg, P. Sjovall and V. Thiel, *Rapid Communications in Mass Spectrometry*, 2013, **27**, 565-581.
23. Y. Zhou, J. Yao, Y. Ding, J. Yu, X. Hua, J. E. Evans, X. Yu, D. B. Lao, D. J. Heldebrant, S. K. Nune, B. Cao, M. E. Bowden, X. Y. Yu, X. L. Wang and Z. Zhu, *J Am Soc Mass Spectrom*, 2016, **27**, 2006-2013.
24. R. J. P. Corriu, D. Leclercq, P. H. Mutin, J. M. Planeix and A. Vioux, *Organometallics*, 1993, **12**, 454-462.
25. F. Caccavo, P. C. Schamberger, K. Keiding and P. H. Nielsen, *Applied and Environmental Microbiology*, 1997, **63**, 3837-3843.
26. S. Mazumder, J. O. Falkinham, A. M. Dietrich and I. K. Puri, *Biofouling*, 2010, **26**, 333-339.
27. A. Kouzuma, X. Y. Meng, N. Kimura, K. Hashimoto and K. Watanabe, *Applied and Environmental Microbiology*, 2010, **76**, 4151-4157.
28. Y. Yang, Y. Z. Ding, Y. D. Hu, B. Cao, S. A. Rice, S. Kjelleberg and H. Song, *Acs Synthetic Biology*, 2015, **4**, 815-823.

29. M. M. Alves, J. A. M. Vieira, R. M. A. Pereira, M. A. Pereira and M. Mota, *Water Research*, 2001, **35**, 255-263.
30. Y. Shen, H. Zhang, X. Xu and X. Lin, *Bioprocess and Biosystems Engineering*, 2015, **38**, 481-488.
31. E. Marsili, D. B. Baron, I. D. Shikhare, D. Coursolle, J. A. Gralnick and D. R. Bond, *Proceedings of the National Academy of Sciences of the United States of America*, 2008, **105**, 3968-3973.
32. C. Lau, J. Roy, P. Atanassov, P. Chellamuthu and K. Nealson, *Abstracts of Papers of the American Chemical Society*, 2011, **241**.
33. T. Morohoshi, S. Nakazawa, A. Ebata, N. Kato and T. Ikeda, *Bioscience Biotechnology and Biochemistry*, 2008, **72**, 1887-1893.
34. S. Favre-Bonte, T. Kohler and C. Van Delden, *Journal of Antimicrobial Chemotherapy*, 2003, **52**, 598-604.
35. E. J. Lanni, R. N. Masyuko, C. M. Driscoll, J. T. Aerts, J. D. Shrout, P. W. Bohn and J. V. Sweedler, *Analytical Chemistry*, 2014, **86**, 9139-9145.
36. I. de Godos, C. Gonzalez, E. Becares, P. A. Garcia-Encina and R. Munoz, *Applied Microbiology and Biotechnology*, 2009, **82**, 187-194.
37. F. Di Natale, A. Lancia, A. Molino and D. Musmarra, *J Hazard Mater*, 2007, **145**, 381-390.

Key Words: biofilm • Shewanella oneidensis • CP2-1-S1 • SALVI • liquid ToF-SIMS • Toxicity • Molecular Imaging

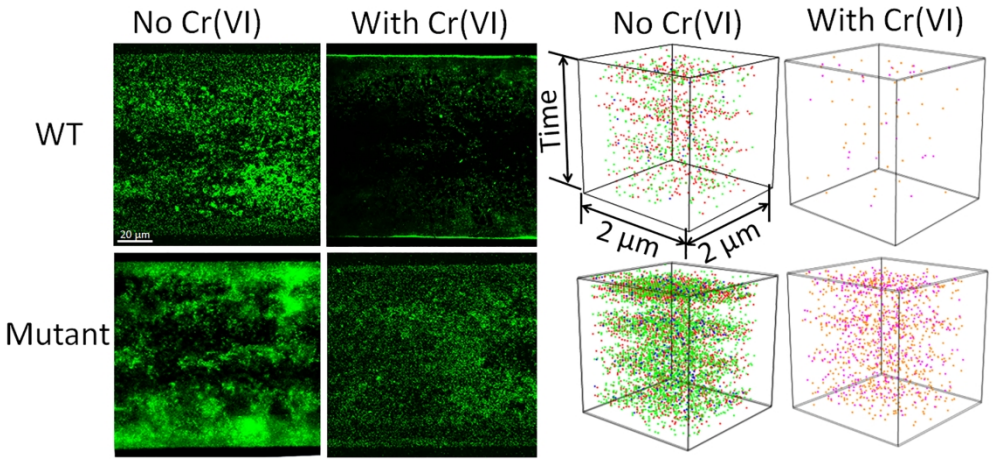

224x101mm (300 x 300 DPI)